Cardiovascular Revascularization Medicine 20 (2019) 480–484

Contents lists available at ScienceDirect

Cardiovascular Revascularization Medicine

Effect of Plaque Composition, Morphology, and Burden on DESolve Novolimus-Eluting Bioresorbable Vascular Scaffold Expansion and Eccentricity — An Optical Coherence Tomography Analysis

Niklas F. Boeder [a], Oliver Dörr [a], Timm Bauer [a], Albrecht Elsässer [b], Helge Möllmann [c], Stephan Achenbach [d], Christian W. Hamm [a], Holger M. Nef [a,*]

[a] University of Giessen, Department of Cardiology, Giessen, Germany
[b] Klinikum Oldenburg, Department of Cardiology, Oldenburg, Germany
[c] St. Johannes Hospital Dortmund, Department of Cardiology, Dortmund, Germany
[d] University of Erlangen, Department of Cardiology, Erlangen, Germany

ARTICLE INFO

Article history:
Received 2 May 2018
Received in revised form 29 July 2018
Accepted 31 July 2018

Keywords:
Novolimus-eluting scaffold
Optical coherence tomography
Plaque composition

ABSTRACT

Objective: This study of patients treated with novolimus-eluting bioresorbable scaffold (BRS) investigated the impact of plaque burden on the acute mechanical performance of the BRS and the short-term outcome.
Methods: A total of 15 patients were enrolled. The following parameters were derived from optical coherence tomography (OCT) during the final pullback: mean and minimum area, residual area stenosis, incomplete strut apposition, tissue prolapse, scaffold expansion index (SEI), scaffold eccentricity index (SEC), symmetry index, strut fracture, and edge dissection. Fibrous plaque (FP) and calcific plaque (CP) characteristics were measured at each 200 μm longitudinal cross-section. The patients were divided into two groups based on their medians of the respective plaque characteristics.
Results: OCT analysis showed a lumen area of 11.4 ± 1.9 mm^2 and a scaffold area of 11.5 ± 2.1 mm^2. The mean eccentricity index overall was 0.65 ± 0.16 and mean symmetry index 0.39 ± 0.25. Statistically, scaffold expansion was not significantly influenced by a greater plaque burden as represented by greater CP area (SEI in group with CP area <0.52 mm^2 84.1% vs. SEI of 86.6% in group with CP area ≥0.52 mm^2, $p = 0.06$), thicker CP (85.7% vs. 85.1%, $p = 0.06$), greater CP arc angle (88.0% vs. 81.7%, $p = 0.08$), and CP being closer to the lumen (84.2% vs. 86.5%, $p = 0.08$). Scaffold expansion was also not significantly influenced by FP burden. The eccentricity of the implanted scaffolds was not dependent on the CP burden. On the other hand, a greater FP burden favoured a lower eccentricity index, indicating less circular expansion. Thus, greater FP area, FP thickness, and FP arc angle resulted in a more eccentric scaffold expansion.
Conclusion: In contrast to previously studied BRS, the expansion and eccentricity characteristics of the novolimus-eluting scaffold did not show the strong dependency of plaque composition, morphology, and burden. As assessed by OCT, only eccentricity was significantly affected by the FP burden. A greater FP plaque arc in our cohort and device-specific properties, e.g. self-correction, may explain the lack of a relationship between plaque, expansion, and eccentricity.

1. Introduction

The bioresorbable scaffolds (BRS) are considered to be the next revolution in coronary stent technology for the treatment of patients with coronary heart disease [1]. BRS are made up of a bioresorbable polymer (poly-L-lactide) backbone coated with an anti-proliferative agent. They offer transient vessel support and are fully resorbed within 24 to 32 months [2]. Following implantation, BRS support the restoration of vasomotor function [3], vascular healing, and positive remodelling [4], thereby potentially overcoming long-term limitations of metallic drug-eluting stents (DES).

The clinical outcome of stent implantation was shown to depend on expansion parameters such as eccentricity and symmetry in the metallic stent era [5,6]. Optical coherence tomography (OCT), a light-based imaging modality with high cross-sectional resolution [7], has gained importance in the daily clinical routine and has been used to assess the expansion characteristics of the Absorb everolimus-eluting BRS

Abbreviations: AS, Area stenosis; BRS, Bioresorbable scaffold; CP, Calcific plaque; DES, Metallic drug-eluting stent; FP, Fibrous plaque; ISA, Incomplete strut apposition; MLA, Minimum lumen area; MLD, Minimum lumen diameter; OCT, Optical coherence tomography; PCI, Percutaneous coronary intervention; QCA, Quantitative coronary angiography; RAS, Residual area stenosis; RVA, Reference vessel area; RVD, Reference vessel diameter.

* Corresponding author at: Klinikstrasse 33, 35392 Giessen, Germany.
E-mail address: holger.nef@me.com (H.M. Nef).

https://doi.org/10.1016/j.carrev.2018.07.030
1553-8389/

(Absorb, Abbott Vascular, Santa Clara, CA, USA). Shaw et al. were able to demonstrate a dependence of expansion and eccentricity on plaque composition, morphology, and burden [8].

Recently, a new novolimus-eluting BRS (DESolve®, Elixir Medical Corporation, Sunnyvale, CA, USA) was approved for clinical use. Given the unique features of the DESolve BRS, including self-correction, the aim of this study was to use OCT to evaluate coronary plaque composition and its influence on the deployment of the DESolve BRS [9–11].

2. Methods

Fifteen consecutive patients undergoing percutaneous coronary intervention (PCI) with a novolimus-eluting BRS under OCT guidance with a final pullback were enrolled in this study. They were treated between April 2014 and March 2015.

The investigation was approved by the ethics committee of the University of Giessen (203/14) and conforms to the principles outlined in the declaration of Helsinki. All patients gave written informed consent.

PCI was performed in accordance with standard clinical practice. The radial approach was pursued when technically feasible. The patients were given unfractionated heparin at 70 U/kg body weight immediately prior to the procedure. Preparation of lesions was commenced with intracoronary application of nitroglycerine. Lesions were then predilated with a non-compliant balloon. BRS and pre-dilatation balloon corresponded in a 1:1 ratio. The novolimus-eluting BRS device (DESolve®, Elixir Medical Corporation, Sunnyvale, CA, USA) was deployed using slow balloon inflation (1 atm over 10 s, 2 atm over 10 s, then 2 s per atm). The recommended pressure was not exceeded and was held for an additional 20–30 s. Post-dilatation following BRS placement was also performed with non-compliant balloons. It was left to the operator's discretion whether or not to use a debulking device.

Frequency domain-OCT was performed using a C7 Dragonfly® intracoronary imaging catheter and the Ilumien Optis system (St. Jude Medical, Inc., Minneapolis, MN, USA). Automatic pullbacks were performed at 36 mm/s during contrast injection at a rate of 3 to 5 ml/s. The pullback was recorded after placing the imaging catheters distally to the treated segments; the recording was continued until either the guiding catheter was reached or the maximum pullback length was completed. Data from the final pullback just before the end of the procedure were used for the analysis in this study.

OCT analysis was performed offline using the LightLab Imaging workstation (St. Jude Medical, Inc.). Longitudinal cross-sections were analysed at 200 μm intervals within the stented lesion and 5 mm proximally and distally to the scaffold (Fig. 1). Measurements were carried out by two independent observers. The following quantitative parameters were determined:

- the scaffold expansion index (SEI), defined as each cross-sectional area divided by the maximal scaffold area
- the scaffold eccentricity index (SEC), computed as the ratio between the minimum and maximum diameters [2,6]
- the symmetry index, defined as the difference between maximum scaffold diameter and minimum scaffold diameter divided by the maximum scaffold diameter
- the percentage of incomplete strut apposition (ISA) at cross-sections, calculated as a percentage of the total number of malapposed struts divided by the total number of struts and the ISA area
- the tissue prolapse area, defined as the projection of tissue into the lumen between struts [12]
- the residual area stenosis (RAS), calculated as [1 – MLA / RVA] were MLA is the minimum lumen area and RVA is the reference vessel area

Plaque characteristics were assessed as previously defined [13]. Calcific plaque (CP) and fibrous plaque (FP) cross-sectional area was measured by tracing the plaque contour (Fig. 2). None of the lesions in the

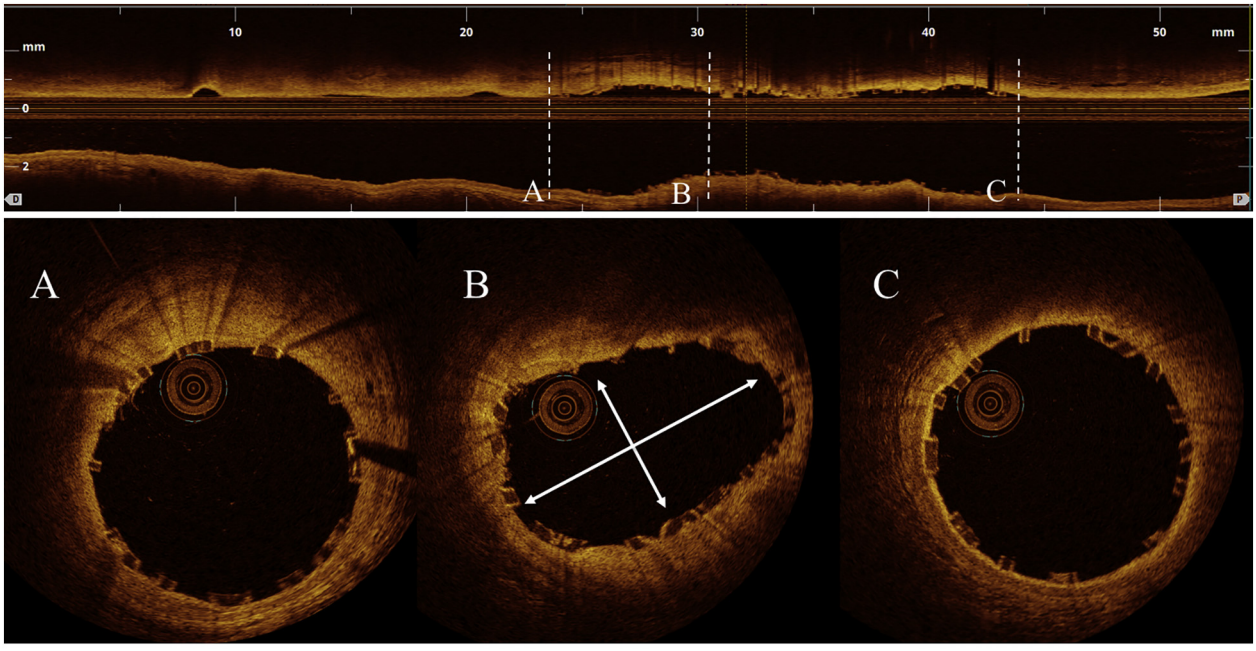

Fig. 1. Longitudinal and cross-sections of OCT pullback showing calculation of minimum eccentricity index and reference vessel area.

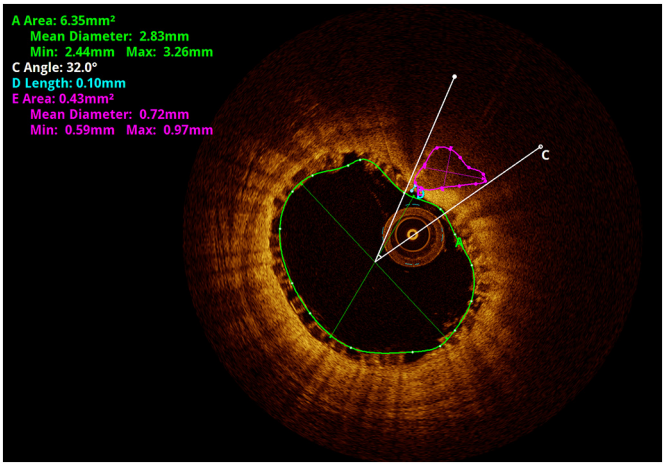

Fig. 2. Example of calcific plaque outlined in pink. CP thickness is indicated in pink. CP arc angle measurement indicated in white. CP depth indicated in aqua.

cohort were homogeneous, lipid-rich plaques, so plaques were either classified as fibrous or calcific based on their major characteristic. CP and FP thickness were measured at the thickest width of plaque. CP and FP arc angles were measured with a protractor and correlated with the angle subtended by the plaque. CP depth is the distance between the adluminal border of the plaque and the lumen border [14]. Any disruption of the vessel luminal surface at the edges of the scaffold with a visible flap (>300 μm) was defined as edge dissection. The patients were divided into two groups based on their medians (Table 1) and analysed with respect to each plaque morphology as previously described [8].

Quantitative coronary angiography (QCA) analysis was performed using offline QCA software (CAAS QCA, Pie Medical Imaging BV, The Netherlands). The analysis was performed post hoc: reference vessel diameter (RVD) was obtained by automatic interpolation as were minimum lumen diameter (MLD), percentage area stenosis (AS), percentage diameter stenosis and lesion length.

Statistical analysis was carried out using IBM SPSS Statistics (SPSS Statistics 23, IBM Deutschland GmbH, Ehningen, Germany). Continuous variables with normal distribution are expressed as means and standard deviations; categorical variables are given as number and percent. Chi-square and Fisher's exact tests were used for comparison of categorical variables, and Student's *t*-test or the Wilcoxon rank-sum test was applied for continuous variables. p values <0.05 were considered statistically significant.

3. Results

A total of 15 patients were enrolled in this study. Baseline characteristics are shown in Table 2. Patients were aged 59.4 ± 8.1 years and 66.7% male. They had a risk profile that is typical for coronary heart disease, including diabetes in 54.3% of the cases. Two-thirds (66.7%) of the enrolled patients had been treated by prior percutaneous coronary intervention (PCI); 40.0% had suffered a myocardial infarction beforehand. Clinical indications were stable angina in 46.7% and acute coronary syndrome in 53.3%. Multiple-vessel disease was present in 80.0%; however, patients enrolled in this study were treated only with a single scaffold in a single lesion. The lesions were predominantly in the left descending arteries (Table 3). None of the lesions included a bifurcation or had ostial involvement. The majority of patients had de novo lesions. QCA parameters are shown in Table 3.

Pre-dilatation was performed prior to scaffold deployment in 86.7%. The balloon for pre-dilatation had a maximum size of 2.9 ± 0.2 mm and was inflated to a maximum of 12.9 ± 3.7 atm (Table 4). Scaffolds were 3.0 mm in diameter and were deployed with a maximum pressure of 17.2 ± 1.6 atm. Non-compliant balloons were used in all cases for post- and pre-dilatation. The balloons for post-dilatation had a maximum diameter of 3.1 ± 0.2 mm and the maximum inflation pressure was 18.3 ± 5.3 atm.

Table 1
Medians of each plaque characteristic measured.

Plaque characteristic	Median
Fibrous plaque area (mm^2)	2.21
Fibrous plaque thickness (mm)	0.52
Fibrous plaque arc angle (°)	244.9
Calcific plaque area (mm^2)	0.55
Calcific plaque thickness (mm)	0.58
Calcific plaque arc angle (°)	34.3
Calcific plaque depth (mm)	0.21

Table 2
Baseline characteristics.

	DESolve (n = 15)
Age (years)	59.4 ± 8.1
Male sex (%)	66.7
Hypertension (%)	100.0
Hyperlipoproteinaemia (%)	100.0
Diabetes (%)	54.3
Current smoker (%)	66.7
Family history (%)	33.3
Prior PCI (%)	66.7
Prior MI (%)	40.0
Left ventricular ejection fraction (%)	52.7 ± 15.8
Clinical indication	
Stable angina (%)	46.7
ACS (%)	53.3
Number of vessels diseased	
1 (%)	20.0
2 (%)	13.3
3 (%)	66.7

Table 3
Angiographic and QCA lesions characteristics.

	DESolve (n = 15)
Target vessel	
LAD (%)	73.3
RCX (%)	6.7
RCA (%)	20.0
De novo lesion (%)	100.0
Total occlusion	0
QCA analysis	
RVD (mm)	2.2 ± 0.3
MLD (mm)	1.1 ± 0.4
AS (%)	70.9
Diameter stenosis (%)	46.8
Lesion length (mm)	9.7 ± 1.7

Table 4
Procedural characteristics.

	DESolve (n = 15)
Pre-dilatation (%)	86.7
Pre-dilatation with NC balloon	100.0
Max. diameter balloon pre-dilatation (mm)	2.9 ± 0.2
Max. pre-dilatation balloon length (mm)	14.3 ± 2.5
Max. pre-dilatation balloon inflation (atm)	12.9 ± 3.7
Scaffold deployment pressure (atm)	17.2 ± 1.6
Post-dilatation (%)	86.7
Post-dilatation with NC balloon	100.0
Max. post-dilatation balloon diameter (mm)	3.1 ± 0.2
Max. post-dilatation balloon length (mm)	14.2 ± 2.6
Max. post-dilatation balloon inflation (atm)	18.3 ± 5.3

Table 5
Optical coherence tomography findings.

	DESolve (n = 15)
Mean scaffold area (mm^2)	6.17 ± 0.64
Mean scaffold diameter (mm)	2.80 ± 0.17
Minimum scaffold diameter (mm)	2.52 ± 0.15
Maximum scaffold diameter (mm)	3.08 ± 0.16
Minimal lumen area (mm^2)	6.05 ± 0.80
Percentage RAS (%)	20.0 ± 4.9
Scaffold with RAS >30% (%)	13.3
Mean eccentricity index	0.83 ± 0.06
Minimum eccentricity index	0.66 ± 0.09
Symmetry index	0.37 ± 0.08
ISA	
ISA area (mm^2)	0.76 ± 2.71
Percentage of malapposed struts (%)	1.43
Prolapse area (mm^2)	2.63 ± 5.20
Strut fracture (%)	6.7
Edge dissection	
Proximal edge (%)	6.7
Distal edge (%)	0

OCT findings are summarized in Table 5. A total of 270 cross-sections and 2979 struts were analysed. The mean scaffold diameter was 2.80 ± 0.17 mm, and the lumen area was calculated to be 6.05 ± 0.80 mm^2. The mean RAS was 20.0%. The mean eccentricity index was computed to be 0.83 ± 0.06. The percentage of malapposed struts was 1.43 ± 0.76%, and the prolapse area was 2.63 ± 5.20 mm^2. OCT revealed strut fractures in 6.7%. Edge dissections were only found at the proximal end (6.7%).

Greater plaque burden, expressed by greater CP area is statistically not associated with a significant increase in scaffold expansion. SEI in group with CP area <0.52 mm^2 computes to be 84.1% vs. 86.6% in the group with SEI ≥0.52 mm^2 ($p = 0.06$). This association holds true for thicker CP (85.7% vs. 85.1%, $p = 0.06$), greater CP arc angle (88.0% vs. 81.7%, $p = 0.08$), and CP being closer to the lumen (84.2% vs. 86.5%, $p = 0.08$). Scaffold expansion was also not significantly influenced by FP burden, expressed as greater FP area. SEI in the group with FP area <1.95 mm^2 computed to be 88.4% vs. 87.6% in the group with FP area ≥1.95 mm^2 ($p = 0.07$). There was, furthermore, no statistically significance in scaffold expansion in dependence of thicker FP (85.6% vs. 89.6%, $p = 0.06$), and greater FP arc angle (90.5% vs. 84.4, $p = 0.05$).

Eccentricity showed no statistically dependency on greater plaque burden expressed by greater CP area. SEC in group with CP area <0.52 mm^2 computes to be 0.82 vs. 0.79 in the group with SEC ≥0.52 mm^2 ($p = 0.08$). This holds true for CP thickness (0.80 vs. 0.81, $p = 0.08$), the CP arc angle (0.82 vs. 0.78, $p = 0.08$), and the distance to the lumen (0.77 vs. 0.84, $p = 0.09$). On the other hand, lower eccentricity index – indicating a less circular expansion – were associated by greater FP burden (Table S1). FP area, expressing FP burden, showed a SEC of 0.86 in group with FP area <1.95 mm^2 and of 0.84 in the group with FP area ≥1.95 mm^2. This difference was statistically significant ($p = 0.03$). This effect was subsequently seen for FP thickness ($p = 0.04$) and FP arc angle ($p = 0.03$). Results are summarized in Table S1.

No adverse cardiac events (scaffold thrombosis, death, target lesion revascularization, target lesion failure) occurred during the hospital stay or within the ensuing 30-day post-procedural period.

4. Discussion and limitations

It has been shown that BRS expansion and eccentricity in patients who are treated with Absorb® BRS are significantly impacted by the coronary artery plaque composition, morphology, and burden [8]. However, it is unclear whether these observations apply to patients implanted with a novolimus-eluting BRS (DESolve® BRS). To obtain optimal BRS implantation, it is crucial to understand aspects of underlying plaque morphologies, particularly how individual lesion characteristics may play a role. Our study is the first OCT study to investigate the impact of plaque burden on the acute mechanical performance and short-term outcome in patients treated with DESolve® BRS.

The patient population selected for the study fulfilled the criteria for the implantation of BRS: they were relatively young (59 ± 8.1 years), had a short history of coronary heart disease, and 40% had suffered a prior myocardial infarction. Approximately two-thirds had had a prior PCI. They comprised the typical cardiovascular risk profile, including the presence of diabetes (54%) and smoking (66.7%).

In our study, DESolve® BRS were implanted with good acute results, as demonstrated by imaging parameters [12,15]. These imaging parameters address the deployment of the scaffolds, and are derived from intravascular ultrasound methods that evaluate acute procedural results and long-term outcomes [16,17]. They demonstrate here that a MLA in the final OCT pullback smaller than 5 mm^2 or a RAS >20% increase the risk of stent thrombosis [5]. The mean residual stenosis in our population was 20%, which therefore met this criterion. Furthermore, our data show that the expansion was not significantly limited by CP area, thickness, arc angle, and distance from the lumen. On the other hand, a greater FP burden led to a lower eccentricity index, indicating less circular expansion. Thus, greater FP area, FP thickness, and FP arc angle resulted in a more eccentric scaffold expansion. This is in contrast with the results of Shaw et al. [8], who showed a dependence of expansion on the CP and FP plaque burden after Absorb® deployment. Whereas the expansion inversely correlated with CP burden, a greater FP burden resulted in a greater BRS expansion. In particular, the MLA indicates appropriate expansion. It was shown that the MLA be improved by aggressive plaque modification with 1:1 pre-dilatation [18]. Pre-dilatation was performed during 87% of the interventions in our cohort. Post-dilatation, on the other hand, does not seem to improve the expansion [18]; however, no randomised data are available supporting this observation. Currently, post-dilatation is strongly recommended whenever further optimisation is required. In our cohort, post-dilatation was performed in 87% of the cases. The preparation and post-BRS-deployment management in the aforementioned study by Shaw et al. [8] was not detailed; therefore, the diverging results could be explained by different methods of lesion preparation. This would indicate that a careful pre-dilatation can overcome the negative impact of CP plaque burden on the BRS implantation result, taking into consideration that only the median CP arc angle but not CP area, CP thickness, or CP depth is slightly smaller in our cohort compared with the patients studied by Shaw et al. [8]. A second aspect that might account for the different results may be the different BRS device used. The DESolve® has a self-expanding property that might have positively contributed to the result in our study cohort. Overall, our results indicate that scaffold expansion is reasonable, with an average SEI of 86.5%.

The assessment of geometrical parameters by OCT during final pullback revealed a mean eccentricity index of 0.83 ± 0.06. The MUSIC study demonstrated a favourable angiographic result at six-month follow-up for an eccentricity value of 0.70 [19]. Brugaletta et al. [2], who also examined only patients treated with a 3.0 mm BRS, documented an eccentricity index of 0.85 ± 0.08. Therefore, our own results agree well with values in the literature. This also holds true for the symmetry index measured in our study (0.37 ± 0.08). The symmetry index gives additional insight into the shape of the scaffolds: if it is near zero, the scaffold is thought to be similar throughout the entire scaffold length [2]. In our cohort, CP area, CP thickness, arc angle, and less distance to the lumen did not adversely influence the eccentricity of the implanted scaffolds. However, greater fibrous plaque burden was associated with a lower eccentricity index. Greater FP area, FP thickness, and FP arc angle resulted in a more eccentric and less circular scaffold expansion. FP was typically found as circumferential clasps. The median FP arc angle in our cohort was calculated to be 250°, which was larger than that in the study conducted by Shaw et al. [6]. Median FP area and thickness, which were smaller in our cohort, still significantly influenced the BRS eccentricity. Softer, lipid-rich plaques exhibit lower dilation resistance during stenting in PCI patients [20]; thus, both the

greater circumferential extent of FP as well as a slightly different plaque composition may have influenced the deployment behaviour of the DESolve® compared to the Absorb®.

After the deployment of BRS, tissue can prolapse through the struts. In our population, the prolapse area was not clinically significant, as mean and minimum lumen diameters were not affected. The percentage of malapposed struts and the area of incomplete strut apposition were also negligible. While the clinical relevance of ISA is unclear [21,22], it is assumed that it can lead to stent-related effects and increase the rate of major adverse cardiac events [23]. Malapposed struts may disrupt laminar flow and activate platelets due to high shear stress, ultimately promoting thrombotic events. The clinical relevance of procedural OCT findings needs further investigation. Until then, BRS implantation should include an invasive imaging modality, e.g. OCT, to optimise deployment [24].

There are several limitations inherent to this study. The protocols used for lesion preparation, scaffold deployment, and post-dilation were the same for all operators contributing to the study; however, potential discrepancies in operator decisions that may have affected the final acute mechanical result cannot be excluded. Furthermore, the sample size of the study was small and OCT pullbacks prior to scaffold deployment were not available.

5. Conclusions

This is the first OCT study to investigate the impact of plaque composition, morphology, and burden on acute mechanical performance and short-term outcome in patients who were treated with DESolve® BRS. In general, DESolve® BRS were implanted with good acute results. In contrast to previously studied BRS, the expansion and eccentricity characteristics of the novolimus-eluting scaffold did not show the strong dependency of plaque composition, morphology, and burden. As assessed by OCT, only eccentricity was significantly affected by the FP burden. A greater FP plaque burden and device-specific properties such as self-correction may explain the effects on eccentricity and the lack of a correlation between CP or FP plaque burden and the scaffold expansion index.

Supplementary data to this article can be found online at https://doi.org/10.1016/j.carrev.2018.07.030.

Acknowledgment

The authors thank Elizabeth Martinson, Ph.D., for editorial assistance.

Funding

No funding.

Conflict of interest statement

Holger Nef received speaking honoraria and an institutional research grant from Elixir Medical (Elixir Medical Corporation, Sunnyvale, CA, USA). All other authors have no potential conflict of interest. There are no relationships with industry regarding this study.

References

[1] Wiebe J, Nef HM, Hamm CW. Current status of bioresorbable scaffolds in the treatment of coronary artery disease. J Am Coll Cardiol 2014;64:2541–51.
[2] Brugaletta S, Gomez-Lara J, Diletti R, Farooq V, van Geuns RJ, de Bruyne B, et al. Comparison of in vivo eccentricity and symmetry indices between metallic stents and bioresorbable vascular scaffolds: insights from the ABSORB and SPIRIT trials. Catheter Cardiovasc Interv 2012;79:219–28.
[3] Roura G, Homs S, Ferreiro JL, Gomez-Lara J, Romaguera R, Teruel L, et al. Preserved endothelial vasomotor function after everolimus-eluting stent implantation. EuroIntervention 2015;11:643–9.
[4] Costopoulos C, Naganuma T, Latib A, Colombo A. Looking into the future with bioresorbable vascular scaffolds. Expert Rev Cardiovasc Ther 2013;11:1407–16.
[5] Fujii K, Carlier SG, Mintz GS, Yang YM, Moussa I, Weisz G, et al. Stent underexpansion and residual reference segment stenosis are related to stent thrombosis after sirolimus-eluting stent implantation: an intravascular ultrasound study. J Am Coll Cardiol 2005;45:995–8.
[6] Otake H, Shite J, Ako J, Shinke T, Tanino Y, Ogasawara D, et al. Local determinants of thrombus formation following sirolimus-eluting stent implantation assessed by optical coherence tomography. JACC Cardiovasc Interv 2009;2:459–66.
[7] Ferrante G, Presbitero P, Whitbourn R, Barlis P. Current applications of optical coherence tomography for coronary intervention. Int J Cardiol 2013;165:7–16.
[8] Shaw E, Allahwala UK, Cockburn JA, Hansen TC, Mazhar J, Figtree GA, et al. The effect of coronary artery plaque composition, morphology and burden on Absorb bioresorbable vascular scaffold expansion and eccentricity - a detailed analysis with optical coherence tomography. Int J Cardiol 2015;184:230–6.
[9] Abizaid A, Costa RA, Schofer J, Ormiston J, Maeng M, Witzenbichler B, et al. Serial multimodality imaging and 2-year clinical outcomes of the novel DESolve novolimus-eluting bioresorbable coronary scaffold system for the treatment of single de novo coronary lesions. JACC Cardiovasc Interv 2016;9:565–74.
[10] Boeder NF, Koepp T, Dorr O, Bauer T, Mattesini A, Elsasser A, et al. A new novolimus-eluting bioresorbable scaffold for large coronary arteries: an OCT study of acute mechanical performance. Int J Cardiol 2016;220:706–10.
[11] Nef H, Wiebe J, Boeder N, Dorr O, Bauer T, Hauptmann KE, et al. A multicenter post-marketing evaluation of the Elixir DESolve® Novolimus-eluting bioresorbable coronary scaffold system: first results from the DESolve PMCF study. Catheter Cardiovasc Interv 2018.
[12] Tearney GJ, Regar E, Akasaka T, Adriaenssens T, Barlis P, Bezerra HG, et al. Consensus standards for acquisition, measurement, and reporting of intravascular optical coherence tomography studies: a report from the International Working Group for Intravascular Optical Coherence Tomography Standardization and Validation. J Am Coll Cardiol 2012;59:1058–72.
[13] Yabushita H, Bouma BE, Houser SL, Aretz HT, Jang IK, Schlendorf KH, et al. Characterization of human atherosclerosis by optical coherence tomography. Circulation 2002;106:1640–5.
[14] Matsumoto M, Yoshikawa D, Ishii H, Hayakawa S, Tanaka M, Kumagai S, et al. Morphologic characterization and quantification of superficial calcifications of the coronary artery—in vivo assessment using optical coherence tomography. Nagoya J Med Sci 2012;74:253–9.
[15] Gomez-Lara J, Diletti R, Brugaletta S, Onuma Y, Farooq V, Thuesen L, et al. Angiographic maximal luminal diameter and appropriate deployment of the everolimus-eluting bioresorbable vascular scaffold as assessed by optical coherence tomography: an ABSORB cohort B trial sub-study. EuroIntervention 2012;8:214–24.
[16] Costa MA, Angiolillo DJ, Tannenbaum M, Driesman M, Chu A, Patterson J, et al. Impact of stent deployment procedural factors on long-term effectiveness and safety of sirolimus-eluting stents (final results of the multicenter prospective STLLR trial). Am J Cardiol 2008;101:1704–11.
[17] Sonoda S, Morino Y, Ako J, Terashima M, Hassan AH, Bonneau HN, et al. Impact of final stent dimensions on long-term results following sirolimus-eluting stent implantation: serial intravascular ultrasound analysis from the sirius trial. J Am Coll Cardiol 2004;43:1959–63.
[18] Brown AJ, McCormick LM, Braganza DM, Bennett MR, Hoole SP, West NE. Expansion and malapposition characteristics after bioresorbable vascular scaffold implantation. Catheter Cardiovasc Interv 2014;84:37–45.
[19] de Jaegere P, Mudra H, Figulla H, Almagor Y, Doucet S, Penn I, et al. Intravascular ultrasound-guided optimized stent deployment. Immediate and 6 months clinical and angiographic results from the Multicenter Ultrasound Stenting in Coronaries Study (MUSIC Study). Eur Heart J 1998;19:1214–23.
[20] Zhou Y, Chen MH, Yang K, Xiong CJ, Chen G, Yang FY, et al. Difference of dilation resistance to coronary stenting between fibrous plaques and lipid-rich plaques. Chin Med J (Engl) 2013;126:4149–53.
[21] Hoffmann R, Morice MC, Moses JW, Fitzgerald PJ, Mauri L, Breithardt G, et al. Impact of late incomplete stent apposition after sirolimus-eluting stent implantation on 4-year clinical events: intravascular ultrasound analysis from the multicentre, randomised, RAVEL, E-SIRIUS and SIRIUS trials. Heart 2008;94:322–8.
[22] Hong MK, Mintz GS, Lee CW, Park DW, Park KM, Lee BK, et al. Late stent malapposition after drug-eluting stent implantation: an intravascular ultrasound analysis with long-term follow-up. Circulation 2006;113:414–9.
[23] Ahn JM, Kang SJ, Yoon SH, Park HW, Kang SM, Lee JY, et al. Meta-analysis of outcomes after intravascular ultrasound-guided versus angiography-guided drug-eluting stent implantation in 26,503 patients enrolled in three randomized trials and 14 observational studies. Am J Cardiol 2014;113:1338–47.
[24] Allahwala UK, Cockburn JA, Shaw E, Figtree GA, Hansen PS, Bhindi R. Clinical utility of optical coherence tomography (OCT) in the optimisation of Absorb bioresorbable vascular scaffold deployment during percutaneous coronary intervention. EuroIntervention 2015;10:1154–9.